Wind and Structures, *Vol. 23, No. 6 (2016) 615-639*
DOI: http://dx.doi.org/10.12989/was.2016.23.6.615

Numerical study on the mitigation of rain-wind induced vibrations of stay cables with dampers

Shouying Li*[1], Teng Wu[2], Shouke Li[3] and Ming Gu[4]

[1]*Hunan Provincial Key Laboratory of Wind Engineering and Bridge Engineering, Hunan University, Changsha 410082, China*
[2]*Department of Civil, Structural and Environmental Engineering, University at Buffalo, State University of New York, Buffalo, NY 14126, USA*
[3]*School of Civil Engineering, Hunan University of Science and Technology, Xiangtan 411201, China*
[4]*State Key Laboratory for Disaster Reduction in Civil Engineering, Tongji University, Shanghai, 200092, China*

(Received April 21, 2015, Revised June 15, 2016, Accepted July 3, 2016)

Abstract. Although the underlying mechanism of rain-wind induced vibrations (RWIVs) of stay cables has not been fully understood, some countermeasures have been successfully applied to mitigating this kind of vibration. Among these, installing dampers near the bridge deck was widely adopted, and several field observations have shown its effectiveness. In this study, the effectiveness of dampers to RWIVs of stay cables is numerically investigated comprehensively by means of finite difference method (FDM). Based on the free vibration analysis of a taut string, it is found that the 3-points triangle scheme, which can be easily implemented in FDM, can offer an excellent approximation of the concentrated damping coefficient (expressed as a Dirac delta function) at the location where the damper is installed. Then, free vibration analysis of a 3-D continuous stay cable attached with two dampers is carried out to study the relationship of modal damping ratio and damping coefficient of the dampers. The effects of orientation of the dampers and cable sag on the modal damping ratio are investigated in detail. Finally, the RWIV response of a 3-D continuous stay cable attached with two dampers is examined. The results indicate that 0.5% of damping ratio is sufficient to reduce the RWIV vibration of the Cable A20 on the No.2 Nanjing Bridge over Yangtze River.

Keywords: 3-D continuous stay cable; Rain-wind induced vibration; dampers; numerical simulations; finite difference method

1. Introduction

Stay cables on cable-stayed bridges due to the low frequency and low structural damping experience several types of wind induced vibrations, such as rain-wind induced vibration (RWIV) (Hikami and Shiraishi 1988), dry galloping (Cheng, Larose *et al*. 2008a, Cheng, Irwin *et al*. 2008b), vortex induced vibration (Zuo, Jones *et al*. 2008, Matsumoto, Yagi *et al*. 2001) and buffeting. Among these cable vibrations, RWIV has a dominant role due to its large amplitude and frequent occurrence.

*Corresponding author, Associate Professor, E-mail: shyli@hun.edu.cn

http://www.techno-press.org/?journal=was&subpage=8 ISSN: 1226-6116 (Print), 1598-6225 (Online)

Many investigators have paid their attentions to the mechanism of RWIVs of stay cables by means of field observations (Hikami and Shiraishi 1988, Matsumoto, Shirato *et al*. 2003, Chen, Wang *et al*. 2004, Phelan, Sarkar *et al*. 2006), wind tunnel tests (Hikami and Shiraishi 1988, Flamand 1995, Gu and Du 2005, Wang, Zhou *et al*. 2005, Li, Chen *et al*. 2010, Du, Gu *et al*. 2013), theoretical analyses (Yamaguchi 1990, Gu and Lu 2001, Peil and Nahrath 2003, van der Burgh and Hartono 2004, Xu and Wang 2003, Wilde and Witkowski 2003, Cosentino, Flamand *et al.* 2003, Cao, Tucker *et al.* 2003, Gu, Du *et al*. 2009, Li, Chen *et al*. 2013, Wu, Kareem *et al*. 2013, Li, Chen *et al*. 2014) and CFD simulations (Li and Gu 2006, Robertson, Taylor *et al*. 2010). Currently, two types of explanations on the mechanism of RWIVs of stay cables have been advanced. The first, shared by most investigators, postulates that the rivulet formed on the upper surface of the cable, which alters the flow around the cable, is the key factor for the onset and sustenance of RWIVs. The second viewpoint was proposed by Matsumoto, Saitoh *et al*. (1995), which, based on the field observations and wind tunnel tests, focused on the role of axial flow along the cable axis in RWIVs.

Although the underlying mechanism of RWIVs of stay cables has not been fully understood, some countermeasures, for example, installing dampers near the bridge deck (Chen, Wang *et al*. 2004), changing the surface configuration of stay cable (Bosdogianni and Olivari 1996, Flamand 1995, Gu and Du 2005) and cable cross tie (Virlogeux 1998, Yamaguchi and Fujino 1998) were proposed to mitigate this type of violent vibration. Among these countermeasures, installing dampers near the bridge deck was widely used and showed its effectiveness to control the RWIVs of stay cables. Virlogeux (1998) pointed out that RWIVs of stay cables can be well mitigated when the damping ratio is higher than 0.5%. The results in Chen, Wang *et al*. (2004) where the MR Dampers was installed on the Dongting Lake Bridge in China suggested that a damping ratio of 0.5~1.2% was sufficient to reduce the RWIVs of stay cables.

Free vibration analysis is usually utilized as a convenient approach to investigate the modal damping produced by the dampers. Based on the study of a taut cable, Pacheco, Fujino (1993) proposed a universal curve to describe the relationship between the modal damping ratios and damping coefficients of dampers by using numerical analysis. This universal curve is extremely useful to facilitate the design of dampers. Later, Krenk (2000) and Main and Jones (2002) successfully obtained a simple analytical form of the universal curve for a taut cable which is the same with the results in Pacheco, Fujino (1993). Tabatabai and Mehrabi (2000) developed a finite difference formulation to study the damping of stay cable with the consideration of the effects of cable sag and cable bending stiffness. Main and Jones (2007) studied the effects of bending stiffness on the damping based on the tensioned beams with intermediate viscous dampers. Fujino and Hoang (2008) analytically derived the asymptotic formulas for the modal damping ratio of a general cable, where the effects of sag, flexural rigidity of the cable and the stiffness of the damper support were discussed. Yu and Xu (1998) and Xu and Yu (1998) conducted both the free and forced vibration analyses of an inclined sag cable equipped with discrete oil dampers by utilizing a so-called hybrid method, where cable sag, cable inclination, damper direction and damper stiffness were considered. In the force vibration analysis, the uniformly distributed harmonic loads were discussed.

In this study, the effectiveness of dampers for mitigating the RWIVs of stay cables is investigated from the viewpoint of numerical simulation by means of Finite Difference Method (FDM). In order to implement the concentrated damping coefficient of the dampers in FDM, five types of distributed damping coefficients are discussed. Their effectiveness is comprehensively studied based on the free vibration analysis of a horizontal taut string model to obtain the optimal

damping coefficient distribution. Then, free vibration analysis of a 3-D continuous stay cable attached with two dampers, in which cable sags and orientations of cable and dampers are taken into account, is carried out to investigate the modal damping ratio provided by the dampers. The effects of cable sag and orientation of dampers on the modal damping ratio are investigated in detail. Finally, based on the theoretical model developed by Gu (2009), the effectiveness of dampers for mitigating the RWIVs of stay cables is discussed.

2. Approximation of the damper's concentrated damping coefficient in FDM

Installing a damper on stay cable will lead to a concentrated damping coefficient. Consequently, Dirac delta function δ would arise in the equations of motion governing the stay cable attached with dampers for the concentrated damping coefficient at the point where the dampers were installed. To accurately implement the Dirac delta function in the FDM, five types of distributed damping coefficients are discussed in the study to obtain the best approximation of the concentrated damping coefficient.

In such a case, a taut string model is first adopted to simulate the stay cable as a simplified version to highlight the discussion of the numerical approximation of the concentrated damping coefficient. A coordinate system ox, in which the original point is at the left endpoint of the taut string, is established, as shown in Fig. 1. The equation of motion governing the taut string could be expressed as (Tikhonov and Samarskii 1963)

$$T\frac{\partial^2 v(x,t)}{\partial x^2}=M\frac{\partial^2 v(x,t)}{\partial t^2}+[c\delta(x-x_c)+c_1]\frac{\partial v(x,t)}{\partial t} \tag{1}$$

which $v(x, t)$ is the displacement perpendicular to cable axis; L is the length of the taut string; T is the axial tension; M is the mass per unit length; c_1 is the structural distributed damping coefficient per unit length; c is the concentrated damping coefficient of the damper; x_c is the distance between the damper and the left endpoint; $\delta(x\text{-}x_c)$ is the Dirac delta function, which can be written as

$$\begin{cases}\int_{x_c^-}^{x_c^+}\delta(x-x_c)dx=1\\ \delta(x-x_c)=0 \qquad x\neq x_c\end{cases} \tag{2}$$

By using variables separation method, $v(x, t)$ in Eq. (1) could be expressed as

$$v(x,t)=V(x)e^{\lambda t} \tag{3}$$

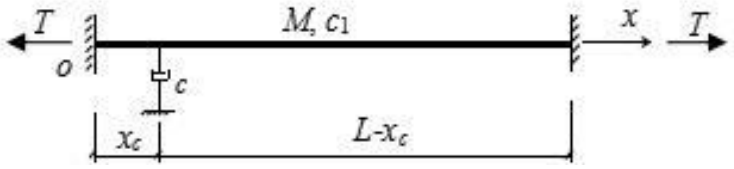

Fig. 1 Taut string attached with damper

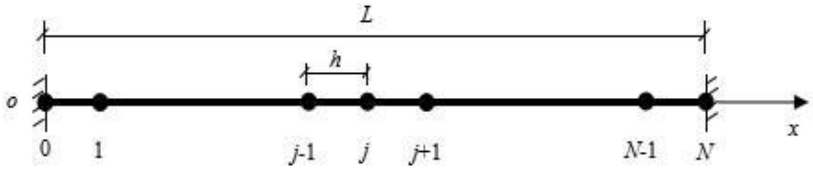

Fig. 2 Discretization of the taut string in space

which

$$\lambda = -\omega\xi \pm \bar{i}\,\omega\sqrt{1-\xi^2} \tag{4}$$

where ω and ξ are natural frequency and modal damping ratio of stay cable, respectively.

Substituting Eq. (3) into Eq. (1), one obtains

$$-T\frac{d^2V(x)}{dx^2} + \lambda^2 MV(x) + \lambda[c\delta(x-x_c)+c_1]V(x) = 0 \tag{5}$$

FDM is adopted to solve Eq. (5). The taut string is uniformly divided into N segments in space, as shown in Fig. 2. Node numbers are 0 to *N* from left to right endpoint. The distance between adjacent nodes is $h = L/N$. The damper is installed at Node *i*.

$d^2V(x_j)/dx^2$ at Nodes 1~*N*-1 can be expressed as,

$$\begin{cases} \dfrac{d^2V(x_1)}{dx^2} = \dfrac{1}{h^2}(-2V_1 + V_2) \\ \dfrac{d^2V(x_j)}{dx^2} = \dfrac{1}{h^2}(V_{j-1} - 2V_j + V_{j+1}) \qquad j = 2,3,\ldots,N-2 \\ \dfrac{d^2V(x_{N-1})}{dx^2} = \dfrac{1}{h^2}(V_{N-2} - 2V_{N-1}) \end{cases} \tag{6}$$

Substituting Eq. (6) into Eq. (5), characteristic equation is obtained

$$\left\{[K] + \lambda^2[M] + \lambda[C]\right\}\{V\} = 0 \tag{7}$$

in which [*K*], [*M*] and [*C*] are stiffness, mass and damping matrixes, respectively.

$$[K] = -\frac{T}{h^2}\begin{bmatrix} -2 & 1 & 0 & \cdots & 0 & 0 & 0 \\ 1 & -2 & 1 & 0 & \cdots & 0 & 0 \\ 0 & 1 & -2 & 1 & 0 & \cdots & 0 \\ \cdots & \cdots & \cdots & \cdots & \cdots & \cdots & \cdots \\ 0 & \cdots & 0 & 1 & -2 & 1 & 0 \\ 0 & 0 & \cdots & 0 & 1 & -2 & 1 \\ 0 & 0 & 0 & \cdots & 0 & 1 & -2 \end{bmatrix}_{(N-1)\times(N-1)} \tag{8}$$

$$[M]=\begin{bmatrix} M & & & \\ & M & & 0 \\ & & \ddots & \\ & 0 & & M \\ & & & & M \end{bmatrix}_{(N-1)\times(N-1)} \tag{9}$$

Damping matrix [*C*] is difficult to be implemented in FDM as there is an infinite concentrated damping coefficient at Node i, where the damper is installed, as indicated in Eq. (2). The exact distribution of damping coefficient along the taut string axis, including the structural distributed damping coefficient, c1, and the concentrated damping coefficient, c, are described in Fig. 3(a). To solve Eq. (5) by using FDM, the concentrated damping coefficient is approximated by the distributed damping coefficients, which are presented in Figs. 3(b)-3(f). Node i in Figs. 3(b)-3(f) is corresponding to the position where the damper is installed. The selected approximation damping distributions in Figs. 3(b)-3(f) follow 3-points triangle, 5-points triangle, 5-points trapezoid, 3-points cosine, 5-points cosine curves, respectively. The integration areas of the above five curves are equal to the concentrated damping coefficient *c*. Table 1 gives the distributed damping coefficients at Node *i*-1, i and *i*+1.

Based on the above mentioned assumptions, the damping matrix [*C*] could be expressed as

$$[C]=\begin{bmatrix} c_1 & & & & & & & \\ & \ddots & & & & & & \\ & & c_1 & & 0 & & & \\ & & & C_{i-1} & & & & \\ & & & & C_i & & & \\ & & & & & C_{i+1} & & \\ & & 0 & & & & c_1 & \\ & & & & & & & \ddots \\ & & & & & & & & c_1 \end{bmatrix} \tag{10}$$

Table 1 The distributed damping coefficients at node *i*-1, *i* and *i*+1

	$C_{i\text{-}1}$	C_i	C_{i+1}
3-points triangle	c_1	$c_1+\frac{c}{h}$	c_1
5-points triangle	$c_1+\frac{c}{4h}$	$c_1+\frac{c}{2h}$	$c_1+\frac{c}{2h}$
5-points trapezoid	$c_1+\frac{c}{3h}$	$c_1+\frac{c}{3h}$	$c_1+\frac{c}{3h}$
3-points cosine	c_1	$c_1+\frac{\pi c}{4h}$	c_1
5-points cosine	$c_1+\frac{\sqrt{2}\pi c}{16h}$	$c_1+\frac{\pi c}{8h}$	$c_1+\frac{\sqrt{2}\pi c}{16h}$

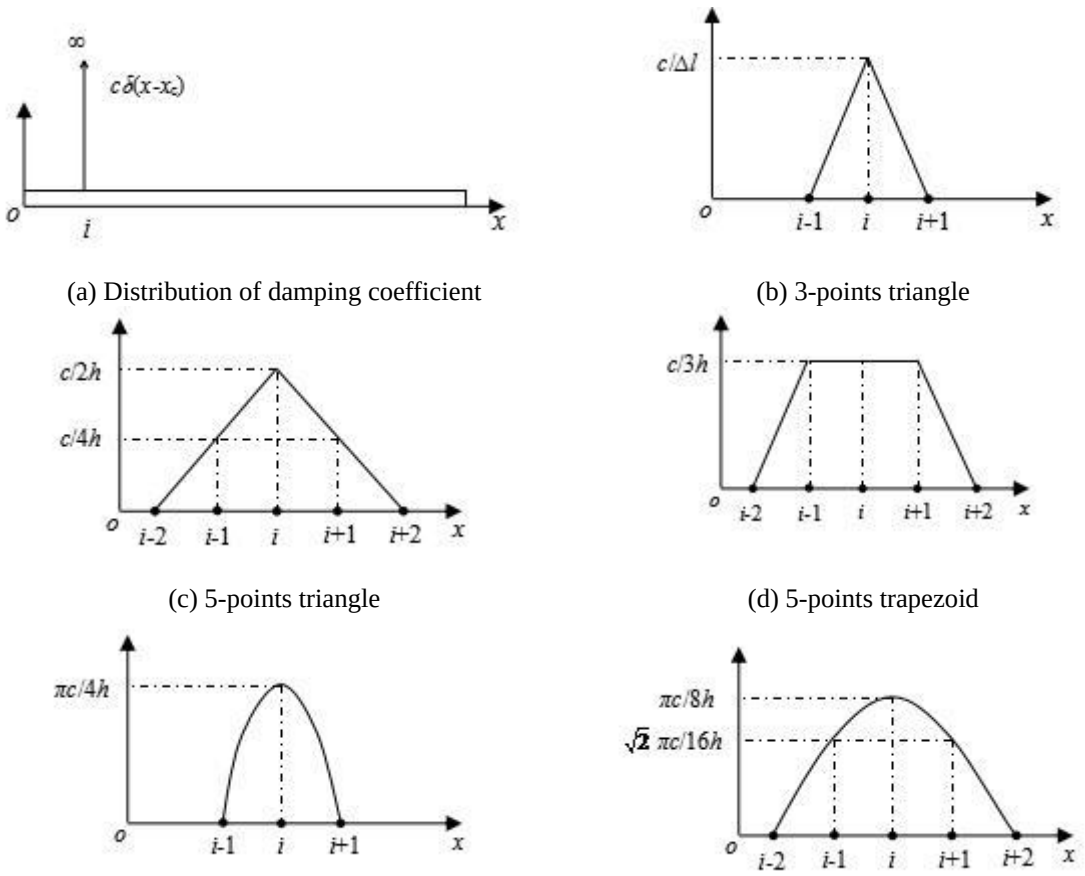

(a) Distribution of damping coefficient (b) 3-points triangle

(c) 5-points triangle (d) 5-points trapezoid

(e) 3-points cosine (f) 5-points cosine

Fig. 3 Distributed approximations for the concentrated damping coefficient

Introducing a state vector

$$\left\{\bar{V}\right\}=\begin{Bmatrix}\{V\}\\ \lambda\{V\}\end{Bmatrix} \tag{11}$$

Eq. (7) can be transformed to a general characteristic value problem

$$\left[A\right]\left\{\bar{V}\right\}=\lambda\left[B\right]\left\{\bar{V}\right\} \tag{12}$$

where

$$\left[A\right]=\begin{bmatrix}\left[K\right] & 0\\ 0 & -\left[M\right]\end{bmatrix} \tag{13}$$

$$[B]=\begin{bmatrix} -[C] & -[M] \\ -[M] & 0 \end{bmatrix} \tag{14}$$

N-1 conjugate eigenvalues λ can be obtained by solving Eq. (12). Substituting λ into Eq. (4), corresponding damping ratio ξ and natural frequency ω can be determined. A computational program is developed by using MATLAB Package. Cable A20 in the No.2 Nanjing Bridge over Yangtze River is taken as an example to analyze its damping ratio due to the damper. The length of the cable is 330.4 m, the mass per unit length is 81.167 kg/m, the section area is 0.0102 m2, the fundamental natural frequency is 0.42 Hz, the horizontal component of axial tension, *H*, is 5545 kN, and the Young's modulus is 1.9×1011 N/m2.

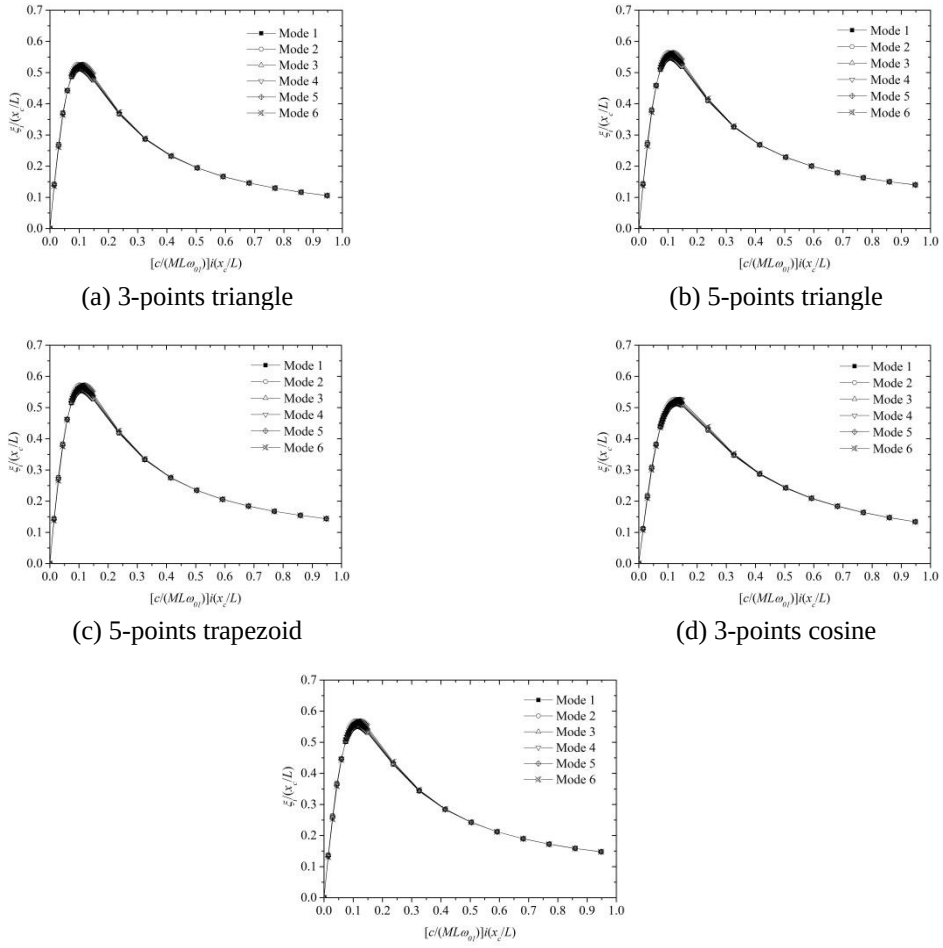

(a) 3-points triangle (b) 5-points triangle

(c) 5-points trapezoid (d) 3-points cosine

(e) 5-points cosine

Fig. 4 Relationship between the damping coefficient of the damper and the realizable modal damping ratio of the first six modes

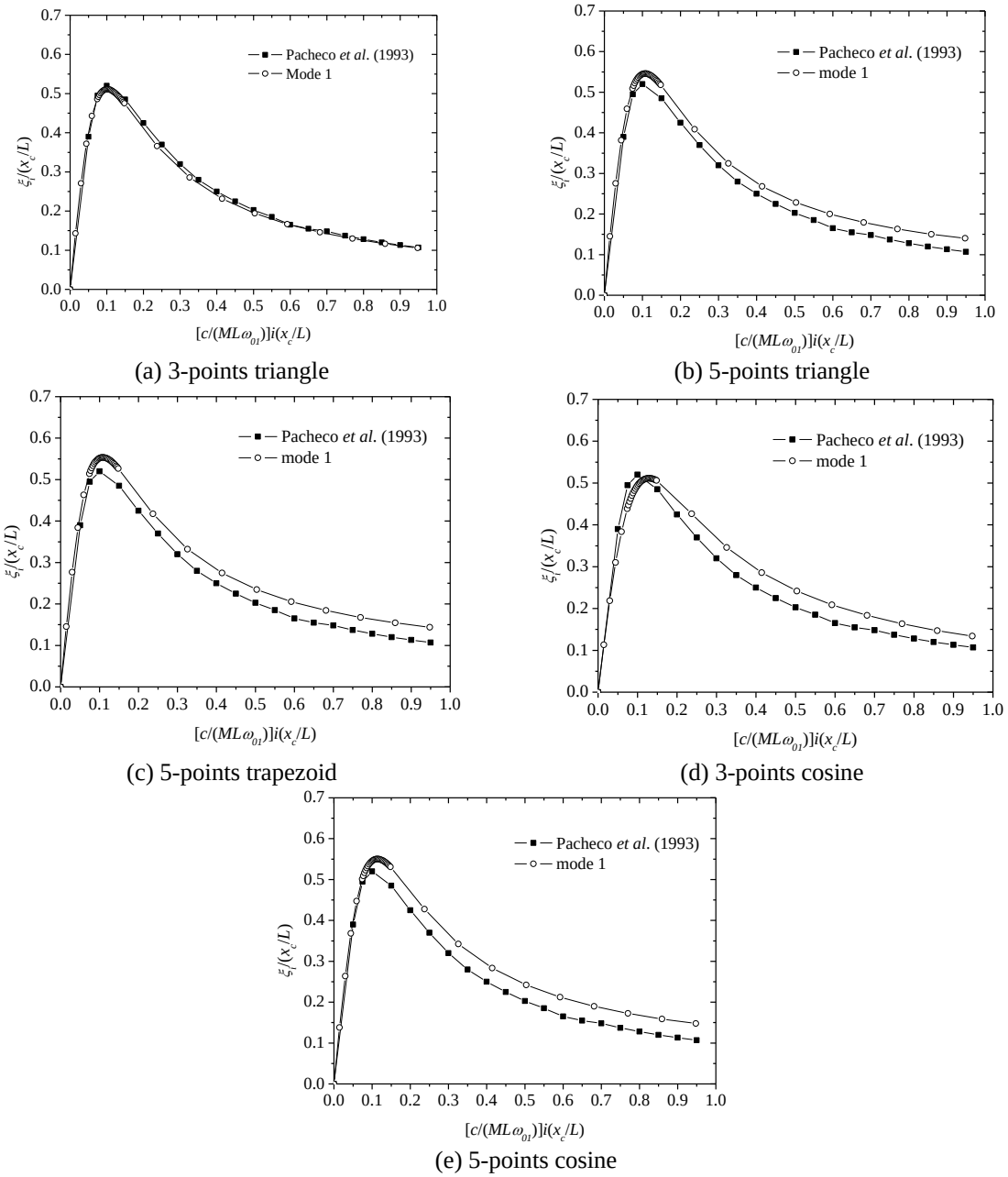

(a) 3-points triangle

(b) 5-points triangle

(c) 5-points trapezoid

(d) 3-points cosine

(e) 5-points cosine

Fig. 5 Comparisons between the first modal damping ratio obtained from five approximate distributed damping coefficients and the theoretical results of Pacheco and Fujino (1993)

Fig. 4 shows the relationship between the damping coefficient of the damper, c, and the realizable modal damping ratio of the first six modes, ξ_i. The longitudinal coordinate is $\xi_i/(x_c/L)$, and the horizontal coordinate is $[c/(ML\omega_{01})i(x_c/L)$, in which ω_{01} is the first natural frequency of

stay cable. From Fig. 4, it can be found that the modal damping ratio curves of the first six modes are reasonably identical with each other for the five approximation distributed damping coefficients.

Fig. 5 presents the comparisons between the first modal damping ratio obtained from five approximation distributed damping coefficients and the theoretical results of Pacheco and Fujino (1993). It can be concluded that the 3-points triangle curve of distributed damping coefficient is the most accurate one to simulate the concentrated damping coefficient among the five selected curves. Hence, 3-points triangle curve of distributed damping coefficient will be used in FDM in this study.

3. Free vibration analysis of 3-D continuous stay cable attached with the dampers

In Section 2, a taut string model is used as there exist classic theoretical results which could be utilized to verify the effectiveness of the damping coefficient approximations. However, the effects of sag should be considered for the real stay cables of the cable-stayed bridges, whose two endpoints are not at the same level. Moreover, in order to mitigate both the in-plane and out-of-plane oscillations of stay cable, two dampers were usually installed.

A 3-D continuous stay cable with an inclined angle of α is considered, as presented in Fig. 6. Two endpoints, the higher-altitude point O on the pylon and the lower-altitude point A on the deck, have a horizontal distance of L and a vertical distance of R. A Cartesian coordinate system, O_{xyz}, is defined, as shown in Fig. 6. Specifically, x and z axes are both horizontal, y axis is vertical, and the stay cable locates in the plane O_{xy}. The orientation of the two dampers is defined by two angles β and γ, where β is the damper inclined angle within the damper plane and γ is the angle between the damper plane and the horizontal plane. Under the action of gravity, the stay cable exhibits a static profile, which can be expressed by a function $y=y(x)$. The equations governing the in-plane motion of the 3-D continuous stay cable attached with two dampers can be written as (Li, Chen *et al*. 2014),

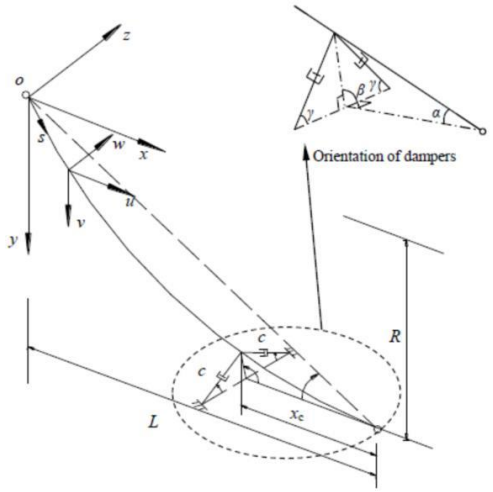

Fig. 6 Diagram of 3-D continuous stay cable attached with two dampers

$$A_1\frac{\partial^2 u}{\partial x^2}+A_2\frac{\partial^2 v}{\partial x^2}+A_3\frac{\partial u}{\partial x}+A_4\frac{\partial v}{\partial x}+f_x(t)\delta[x-(L-x_c)]=M\frac{\partial^2 u}{\partial t^2}+c_1\frac{\partial u}{\partial t} \tag{15}$$

$$A_5\frac{\partial^2 v}{\partial x^2}+A_2\frac{\partial^2 u}{\partial x^2}+A_6\frac{\partial v}{\partial x}+A_4\frac{\partial u}{\partial x}+f_y(t)\delta[x-(L-x_c)]=M\frac{\partial^2 v}{\partial t^2}+c_1\frac{\partial v}{\partial t} \tag{16}$$

in which

$$A_1=\frac{H}{\sqrt{1+y_x^2}}+\frac{EA}{(1+y_x^2)^2} \qquad A_2=\frac{E\,A\,y}{(1+y_x^2)^2} \qquad A_3=-\frac{3E\,A\,y}{(1+y_x^2)^3}\frac{\partial^2 y}{\partial x^2}$$

$$A_4=\frac{EA(1-2y_x^2)}{(1+y_x^2)^3}\frac{\partial^2 y}{\partial x^2} \qquad A_5=\frac{H}{\sqrt{1+y_x^2}}+\frac{EAy_x^2}{(1+y_x^2)^2} \qquad A_6=\frac{EA(2y_x-y_x^3)}{(1+y_x^2)^3}\frac{\partial^2 y}{\partial x^2}$$

where u and v are the dynamic displacement components in the x and y directions, respectively; x_c is the horizontal distance between the dampers and the right (lower) endpoint; E is the Young's modulus of the cable; A is the area of the cable cross section; H is the horizontal component of the axial tension of the cable; y_x is the derivative of cable static profile, $y=y(x)$; $f_x(t)$ and $f_y(t)$ are the damping forces induced by the dampers in x and y directions. $f_x(t)$ and $f_y(t)$ can be obtained from

$$\begin{Bmatrix} f_x \\ f_y \end{Bmatrix}=\begin{bmatrix} -2\sin^2\gamma\cos^2\beta & 2\sin^2\gamma\sin\beta\cos\beta \\ 2\sin^2\gamma\sin\beta\cos\beta & -2\sin^2\gamma\sin^2\beta \end{bmatrix}\times\begin{Bmatrix} c\dfrac{\partial u(L-x_c,t)}{\partial t} \\ c\dfrac{\partial v(L-x_c,t)}{\partial t} \end{Bmatrix} \tag{17}$$

By using variables separation method, $u(x,t)$ and $v(x,t)$ in Eqs. (15) and (16) could be expressed as

$$u=U(x)e^{\lambda t} \tag{18}$$

$$v=V(x)e^{\lambda t} \tag{19}$$

Substituting Eqs. (17)-(19) into Eqs. (15) and (16), one obtains

$$\begin{aligned} &A_1\frac{\partial^2 U(x)}{\partial x^2}+A_2\frac{\partial^2 V(x)}{\partial x^2}+A_3\frac{\partial U(x)}{\partial x}+A_4\frac{\partial V(x)}{\partial x}+\lambda c[-2\sin^2\gamma\cos^2\beta U(L-x_c)+ \\ &2\sin^2\gamma\sin\beta\cos\beta V(L-x_c)]\delta[x-(L-x_c)]=\lambda^2\cdot MU(x)+\lambda\cdot c_1U(x) \end{aligned} \tag{20}$$

$$\begin{aligned} &A_5\frac{\partial^2 V(x)}{\partial x^2}+A_2\frac{\partial^2 U(x)}{\partial x^2}+A_6\frac{\partial V(x)}{\partial x}+A_4\frac{\partial U(x)}{\partial x}+\lambda c[2\sin^2\gamma\sin\beta\cos\beta U(L-x_c) \\ &-2\sin^2\gamma\sin^2\beta V(L-x_c)]\delta[x-(L-x_c)]=\lambda^2 MV(x)+\lambda c_1V(x) \end{aligned} \tag{21}$$

Eqs. (20) and (21) are solved by FDM. The stay cable is divided into N segments, as shown in

Fig. 7. Node numbers are 0 to N from left to right endpoint. The horizontally distance between adjacent nodes is $h = L/N$. Boundary conditions are expressed as

$$U_0(x) = U_N(x) = 0 \ , \ V_0(x) = V_N(x) = 0 \tag{22}$$

According to the results in Section 2, the concentrated damping coefficient of the dampers is approximated by 3-points triangle distributed damping coefficient. Similar to Eq. (5), Eqs. (20) and (21) could be written as

$$\left\{\left[K\right] + \lambda^2\left[M\right] + \lambda\left[C\right]\right\}\left\{V\right\} = 0 \tag{23}$$

in which

$$\left[C\right] = \begin{bmatrix}
c_1 & 0 & 0 & 0 & 0 & 0 & 0 & 0 \\
0 & \ddots & 0 & 0 & 0 & 0 & 0 & 0 \\
0 & 0 & c_1 & 0 & 0 & 0 & 0 & 0 \\
0 & 0 & 0 & c_1 + 2\sin^2\gamma\cos^2\beta\dfrac{c}{h} & -2\sin^2\gamma\sin\beta\cos\beta\dfrac{c}{h} & 0 & 0 & 0 \\
0 & 0 & 0 & -2\sin^2\gamma\sin\beta\cos\beta\dfrac{c}{h} & c_1 + 2\sin^2\gamma\sin^2\beta\dfrac{c}{h} & 0 & 0 & 0 \\
0 & 0 & 0 & 0 & 0 & c_1 & 0 & 0 \\
0 & 0 & 0 & 0 & 0 & 0 & \ddots & 0 \\
0 & 0 & 0 & 0 & 0 & 0 & 0 & c_1
\end{bmatrix}_{2(N-1)\times 2(N-1)}$$

$$\left[M\right] = \begin{bmatrix}
M & & & \\
& M & & 0 \\
& & \ddots & \\
& 0 & & M \\
& & & & M
\end{bmatrix}_{2(N-1)\times 2(N-1)}$$

$$\left[K\right] = -\begin{bmatrix}
\left[B_1\right] & \left[C_1\right] & & & & & & \\
\left[A_2\right] & \left[B_2\right] & \left[C_2\right] & & & & & \\
& \ddots & \ddots & \ddots & & & & \\
& & \left[A_i\right] & \left[B_i\right] & \left[C_i\right] & & & \\
& & & \ddots & \ddots & \ddots & & \\
& & & & \left[A_{N-2}\right] & \left[B_{N-2}\right] & \left[C_{N-2}\right] & \\
& & & & & \left[A_{N-1}\right] & \left[B_{N-1}\right]
\end{bmatrix}$$

$$\{V\}=\left[U_1,V_1,U_2,V_2,\cdots\cdots,U_{N-1},V_{N-1}\right]'$$

$$\left[A_i\right]=\begin{bmatrix}\dfrac{A_1(i)}{h^2}-\dfrac{A_3(i)}{2h} & \dfrac{A_2(i)}{h^2}-\dfrac{A_4(i)}{2h}\\ \dfrac{A_2(i)}{h^2}-\dfrac{A_4(i)}{2h} & \dfrac{A_5(i)}{h^2}-\dfrac{A_6(i)}{2h}\end{bmatrix}$$

$$\left[B_i\right]=\begin{bmatrix}-\dfrac{2A_1(i)}{h^2} & -\dfrac{2A_2(i)}{h^2}\\ -\dfrac{2A_2(i)}{h^2} & -\dfrac{2A_5(i)}{h^2}\end{bmatrix}$$

$$\left[C_i\right]=\begin{bmatrix}\dfrac{A_1(i)}{h^2}+\dfrac{A_3(i)}{2h} & \dfrac{A_2(i)}{h^2}+\dfrac{A_4(i)}{2h}\\ \dfrac{A_2(i)}{h^2}+\dfrac{A_4(i)}{2h} & \dfrac{A_5(i)}{h^2}+\dfrac{A_6(i)}{2h}\end{bmatrix}$$

According to the results in Section 2, the concentrated damping coefficient of the dampers is approximated by 3-points triangle distributed damping coefficient. Similar to Eq. (5), Eqs. (20) and (21) could be written as

$$\left\{\left[K\right]+\lambda^2\left[M\right]+\lambda\left[C\right]\right\}\{V\}=0 \tag{23}$$

which

$$[C]=$$

$$\begin{bmatrix}
c_1 & 0 & 0 & 0 & 0 & 0 & 0 & 0\\
0 & \ddots & 0 & 0 & 0 & 0 & 0 & 0\\
0 & 0 & c_1 & 0 & 0 & 0 & 0 & 0\\
0 & 0 & 0 & c_1+2\sin^2\gamma\cos^2\beta\dfrac{c}{h} & -2\sin^2\gamma\sin\beta\cos\beta\dfrac{c}{h} & 0 & 0 & 0\\
0 & 0 & 0 & -2\sin^2\gamma\sin\beta\cos\beta\dfrac{c}{h} & c_1+2\sin^2\gamma\sin^2\beta\dfrac{c}{h} & 0 & 0 & 0\\
0 & 0 & 0 & 0 & 0 & c_1 & 0 & 0\\
0 & 0 & 0 & 0 & 0 & 0 & \ddots & 0\\
0 & 0 & 0 & 0 & 0 & 0 & 0 & c_1
\end{bmatrix}_{2(N-1)\times 2(N-1)}$$

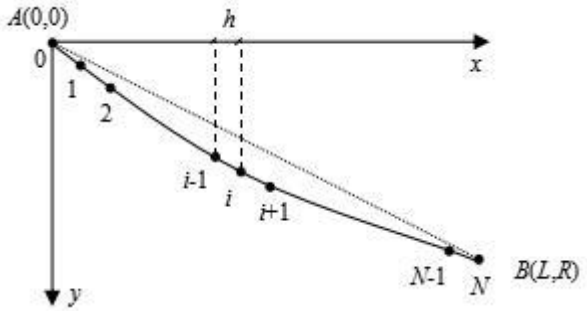

Fig. 7 Discretization of 3-D continuous stay cable attached with dampers

$$[M]=\begin{bmatrix} M & & & \\ & M & & 0 \\ & & \ddots & \\ & 0 & & M \\ & & & & M \end{bmatrix}_{2(N-1)\times 2(N-1)}$$

$$[K]=-\begin{bmatrix} [B_1] & [C_1] & & & & & & \\ [A_2] & [B_2] & [C_2] & & & & & \\ & \ddots & \ddots & \ddots & & & & \\ & & [A_i] & [B_i] & [C_i] & & & \\ & & & \ddots & \ddots & \ddots & & \\ & & & & [A_{N-2}] & [B_{N-2}] & [C_{N-2}] \\ & & & & & [A_{N-1}] & [B_{N-1}] \end{bmatrix}$$

$$\{V\}=\left[U_1,V_1,U_2,V_2,\cdots\cdots,U_{N-1},V_{N-1}\right]'$$

$$[A_i]=\begin{bmatrix} \frac{A_1(i)}{h^2}-\frac{A_3(i)}{2h} & \frac{A_2(i)}{h^2}-\frac{A_4(i)}{2h} \\ \frac{A_2(i)}{h^2}-\frac{A_4(i)}{2h} & \frac{A_5(i)}{h^2}-\frac{A_6(i)}{2h} \end{bmatrix}$$

$$\left[B_i\right]=\begin{bmatrix} -\frac{2A_1(i)}{h^2} & -\frac{2A_2(i)}{h^2} \\ -\frac{2A_2(i)}{h^2} & -\frac{2A_5(i)}{h^2} \end{bmatrix}$$

$$\left[C_i\right]=\begin{bmatrix} \frac{A_1(i)}{h^2}+\frac{A_3(i)}{2h} & \frac{A_2(i)}{h^2}+\frac{A_4(i)}{2h} \\ \frac{A_2(i)}{h^2}+\frac{A_4(i)}{2h} & \frac{A_5(i)}{h^2}+\frac{A_6(i)}{2h} \end{bmatrix}$$

Similar to Eq. (7) in Section 2, Eq. (23) could be solved by introducing a state vector, and the modal damping ratio and natural frequency could be obtained.

Structural parameters of Cable A20 in the No.2 Nanjing Bridge over Yangtze River are used. In addition, cable inclined angle α is 30°. The angle between the damper plane and the horizontal plane, β, is 60°, which means that the damper plane is perpendicular to the cable axis. The angle between the damper and the horizontal line in the damper plane, γ, is 45°. The point where the dampers are installed is 9 m away from the lower endpoint attached on the bridge deck, that is, x_c/L=0.027. Fig. 8 presents the relationship between the damping ratios of the first five modes and the damping coefficients of the two dampers. L_r in Fig. 8 is the distance between two endpoints of the stay cable, and ω_{01} is the first circular frequency of the stay cable, here ω_{01}=2.64 rad/s. It can be found from Fig.8 that the realizable maximum damping ratios of the first five modes are all about 0.53x_c/L, which is identical with the results of the taut string in Section 2. However, the non-dimensional optimal damping coefficient, about 0.09, is slightly smaller than the value of the taut string. This is probably due to that there are two dampers with angle of γ adopted in the 3-D continuous stay cable, which is significantly different from the situation of the taut string.

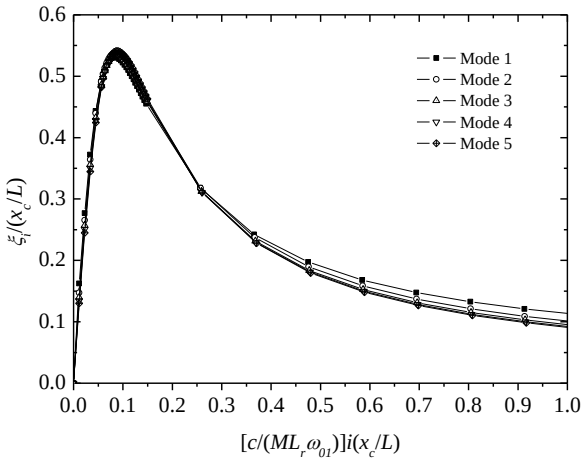

Fig. 8 The relationship between the damping ratios of the first five modes and the damping coefficients of the two dampers

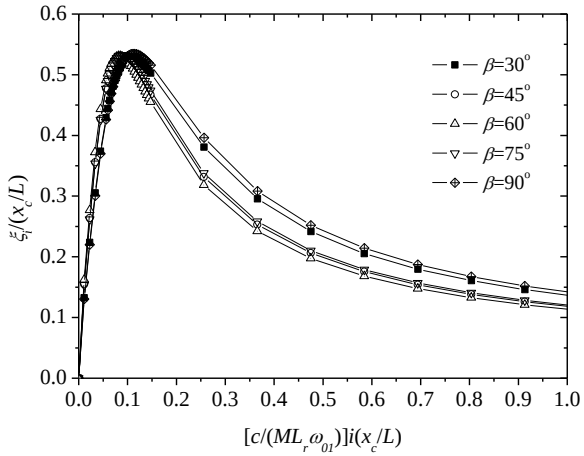

Fig. 9 The relationship between the damping ratio and the damping coefficient of the dampers for different angles β (β=30°, 45°, 60°, 75°, 90°)

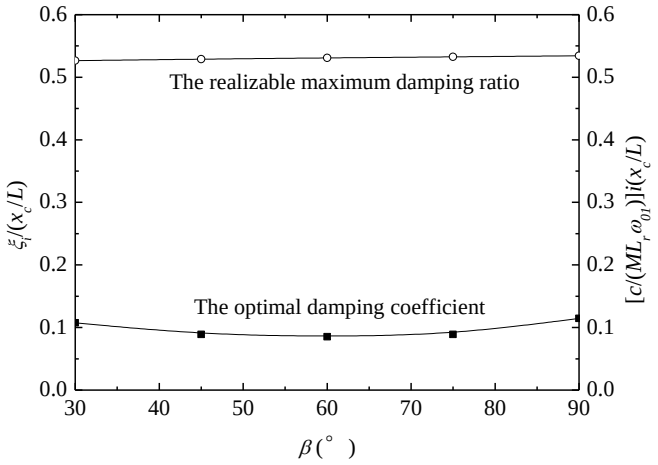

Fig. 10 The realizable damping ratio and it corresponding optimal damping coefficient for different angles β

Fig. 9 shows the relationship between the damping ratio of the first mode and the damping coefficient of the dampers for different angles β (β=30°, 45°, 60°, 75°, 90°), where x_c/L=0.027 and γ=45°. From Fig. 9, it can be found that the realizable maximum damping ratio nearly keeps unchangeable (about $0.53x_c/L$) when the angle between the damper plane and the horizontal plane varies from 30° to 90°. The optimal damping coefficient for β=60°, under which the damper plane is perpendicular to the cable axis, is slightly smaller than those for β=30°, 45°, 75°, 90°, as indicated in Fig. 10.

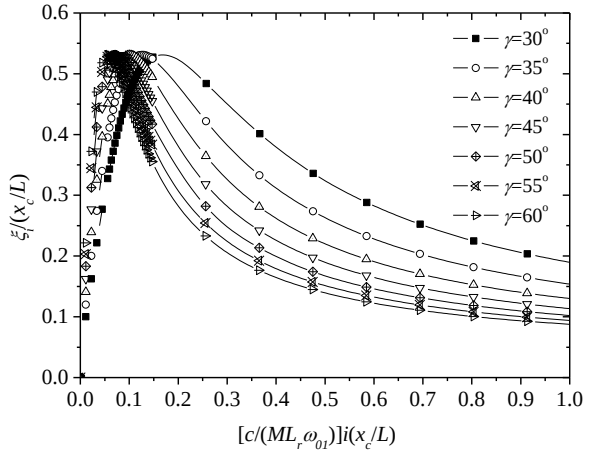

Fig. 11 the relationship between the damping ratio and the damping coefficient of the dampers for different angles γ (γ=30°, 35°, 40°, 45°, 50°, 55°, 60°)

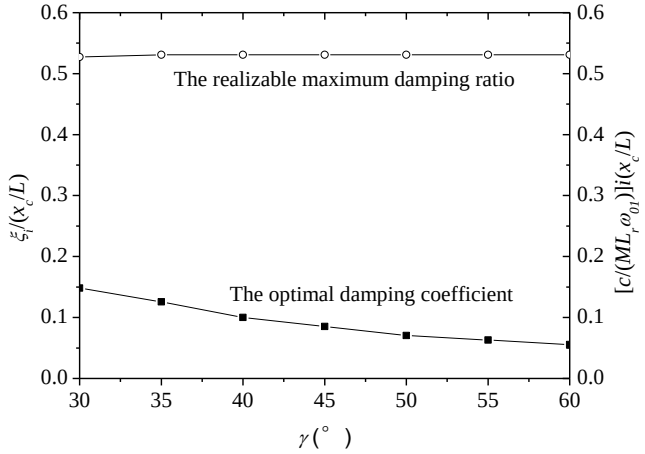

Fig. 12 The realizable damping ratio and it corresponding optimal damping coefficient for different angles γ

Fig. 11 presents the relationship between the damping ratio of the first mode and the damping coefficient of the dampers for different angles γ (γ=30°, 35°, 40°, 45°, 50°, 55°, 60°), where x_c/L=0.027 and β=60°. It can be found from Fig. 11 that the realizable maximum damping ratio is nearly unchangeable (about $0.53x_c/L$) when angle γ varies from 30° to 60°. However, the optimal damping coefficient of the damper increases when the angle γ decreases, as described in Fig. 12. For example, the optimal non-dimensional damping coefficient is 0.148 for γ=30°, while 0.056 for γ=60°. This is because that the components of the damping force decomposed to the cable plane become larger when the angle γ increases.

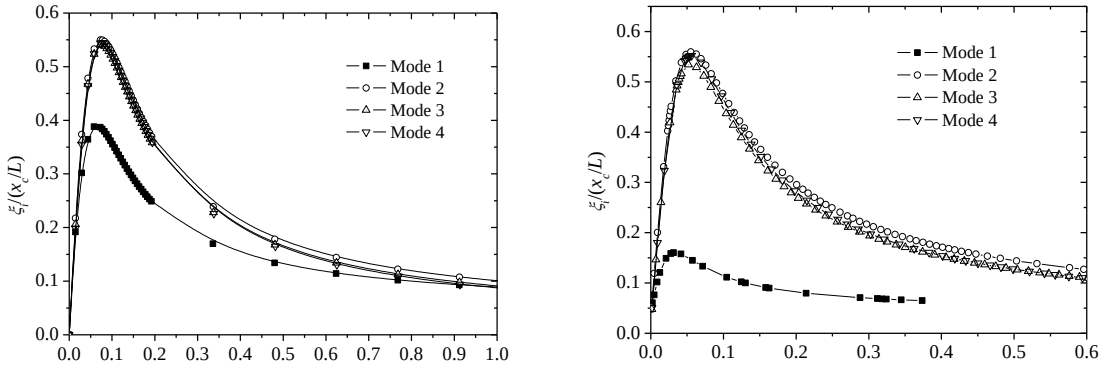

(a) f/Lr=1.3% (b) f/Lr=2.2%

Fig. 13 The relationship between the damping ratio of the first four modes and the damping coefficient of the dampers for different cable sag ratios

Cable sag might affect the effectiveness of the dampers. Figs. 13(a) and 13(b) present the relationship between the damping ratio of the first four modes and the damping coefficient of the dampers for H=2545 kN and 1545 kN, in which x_c/L=0.027, β=60° and γ=45°. The cable sag ratio f/L_r is 0.6%, 1.3% and 2.2% for H=5545, 2545 and 1545kN, respectively. As shown in the figure, the cable sag greatly reduces the maximum realizable damping ratio of the first modes. The maximum realizable damping ratio of the first mode is $0.388x_c/L$ and $0.16x_c/L$ for f/L_r=1.3% and 2.2%, respectively, much smaller than the value of $0.53x_c/L$ for f/L_r=0.6%. On the other hand, cable sag seems to have no significant effects on the maximum realizable damping ratio of the 2nd to 4th modes.

4. Effectiveness of dampers to mitigate RWIVs of stay cables

In Gu (2009), a theoretical model to determine the aerodynamic forces on a 3-D continuous stay cable for RWIV was developed. The aerodynamic force model proposed in Gu (2009) is adopted in this study to analyze the effectiveness of dampers to reduce RWIV. Considering aerodynamic forces acting on the 3-D continuous stay cable in the x and y directions, $F_x(y, t)$ and $F_y(y, t)$, the equation governing the in-plane motion of the stay cable attached with dampers can be written as

$$A_1\frac{\partial^2 u}{\partial x^2}+A_2\frac{\partial^2 v}{\partial x^2}+A_3\frac{\partial u}{\partial x}+A_4\frac{\partial v}{\partial x}+F_x(y,t)+f_x(t)\delta[x-(L-x_c)]=M\frac{\partial^2 u}{\partial t^2}+c_1\frac{\partial u}{\partial t} \tag{24}$$

$$A_5\frac{\partial^2 v}{\partial x^2}+A_2\frac{\partial^2 u}{\partial x^2}+A_6\frac{\partial v}{\partial x}+A_4\frac{\partial u}{\partial x}+F_y(y,t)+f_y(t)\delta[x-(L-x_c)]=M\frac{\partial^2 v}{\partial t^2}+c_1\frac{\partial v}{\partial t} \tag{25}$$

Comparing Eqs. (24) and (25) with Eqs. (15) and (16), the only difference is the aerodynamic forces, $F_x(y, t)$ and $F_y(y, t)$, which can be determined by

$$F_x(y,t) = \frac{1}{2}\rho D U_{rel}^2(y)[C_L(\phi'(y))\cos(\phi(y)) + C_D(\phi'(y))\sin(\phi(y))]\sin\alpha \tag{26}$$

$$F_y(y,t) = -\frac{1}{2}\rho D U_{rel}^2(y)[C_L(\phi'(y))\cos(\phi(y)) + C_D(\phi'(y))\sin(\phi(y))]\cos\alpha \tag{27}$$

in which ρ is the density of air; D is the diameter of stay cable; U_{rel} is the relative wind speed between the approaching flow and the oscillating cable; C_L and C_D are the mean lift and drag coefficients of the cable; ϕ is the angle between the relative wind speed U_{rel} and the horizontal plan; $\phi' = \phi + \beta_0 + \theta$ is the angle between the relative wind speed U_{rel} and the rivulet position,; β_0 and θ are the initial rivulet angle and the rivulet instantaneous position, respectively; α is the inclined angle of stay cable. For a cross section of stay cable, the relation between U, U_{rel}, ϕ, ϕ', β_0 and γ is described in Fig. 14.

The equation of motion of the rivulet in tangential direction can be written as

$$mR\frac{\partial^2\theta}{t^2} + F_0 + c_r R\frac{\partial\theta}{t} = f_\tau(y) + m(\ddot{y} - \ddot{x})\cos(\beta_0 + \theta) - mg\cos\alpha\cos(\beta_0 + \theta) \tag{28}$$

where m and R are the mass per unit length and characteristic size of the rivulet, respectively, F_0 and c_r are the constant damping force and linear damping coefficient between the cable surface and the rivulet; f_τ is the aerodynamic force on the rivulet

$$f_\tau(y) = \frac{1}{2}\rho U_{rel}^2(y)B\left[(c_d(\phi')\sin(\phi(y)) + c_l(\phi')\cos(\phi(y))\right] \tag{29}$$

in which c_d and c_l are the drag and lift coefficients of the rivulet, respectively.

Eqs. (24) and (25) can be discretized in space by FDM as done in Section 3 for Eqs. (20) and (21), and can be written as

$$[M]\frac{d^2\{u\}}{dt^2} + [C]\frac{d\{u\}}{dt} + [K]\{u\} = \{F\} \tag{30}$$

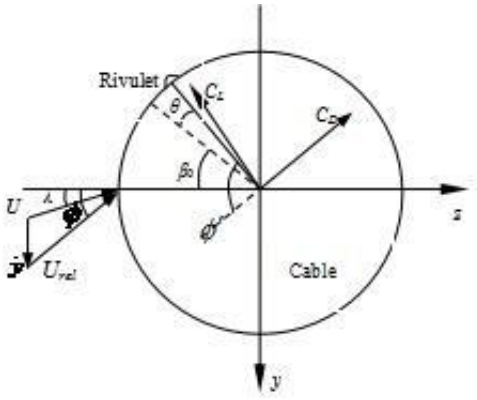

Fig. 14 The relation between U, U_{rel}, ϕ, ϕ', β_0 and θ

where

$$\{u\}=\left[u_1,v_1,\cdots\cdots,u_i,v_i,\cdots\cdots,u_{N-1},v_{N-1}\right]' \tag{31}$$

$$\{F\}=\left[F_x(y_1,t),F_y(y_1,t),\cdots\cdots,F_x(y_{N-1},t),F_y(y_{N-1},t)\right]' \tag{32}$$

Mass matrix [*M*], damping matrix [*C*] and stiffness matrix [*K*] are identical with those given in Section 3. At node *j*, the motion equation of the rivulet can be written as

$$mR\frac{\partial^2\theta_j(t)}{t^2}+F_0+c_rR\frac{\partial\theta_j(t)}{t}=f_\tau+m(\ddot{y}-\ddot{x})\cos(\beta_0+\theta_j)-mg\cos\alpha\cos(\beta_0+\theta_j) \tag{33}$$
$$j=1,2,\ldots,N-1$$

It should be noted that Eq. (30) governing the motion of the cable is coupled with Eq. (33) governing the motion of the rivulet due to the rivulet position θ in Eq. (30) and the cable accelerations ẍ and $\ddot{y}$ in Eq. (33). Linear acceleration method (LAM) is adopted to solve Eqs. (30) and (33) to capture the RWIV responses of stay cable attached with dampers.

Cable A20 in the No.2 Nanjing Bridge over Yangtze River is taken as an example. The cable has a diameter of 11.4 cm and a first natural frequency of 0.42 Hz. The dampers parameters are xc/L=0.027, β=60°, γ=45°. Structural damping ratio of 0.1% for the first mode is adopted, which could be adjusted by structural distributed damping coefficient, c_1. Terrain category *B* of Chinese Code GB50009-2012 is used, in which the mean wind velocity is described as power law. For terrain category *B*, the mean wind velocity at the height of *z*, $U(z)=U_{10}(z/10)0.15$ (U_{10} is the basic wind speed). Gu (2009) found that large amplitude of RWIV on the Cable A20 in the No.2 Nanjing Bridge over Yangtze River without dampers was numerically achieved within the wind speed range of U_d=6.5~8.0 m/s, where U_d is the wind speed at the height of the bridge deck. Fig. 15 presents the relationship between the cable amplitude at mid-point and wind velocity under different damping coefficient of the dampers, including *c*=0, 1×104, 2×104, 1.5×106 and 2×106 N·s/m. It can be found from Fig. 15 that RWIV of stay cable could be well mitigated if the damping coefficient of the damper is reasonably determined, for instance, 2×104≤*c*≤1.5×106 N·s/m.

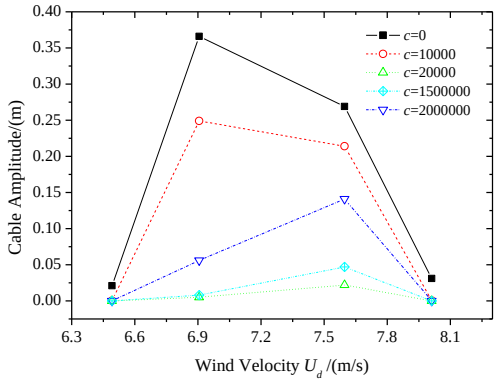

Fig. 15 The relationship between the cable amplitude at mid-point and wind velocity under different damping coefficient of the damper

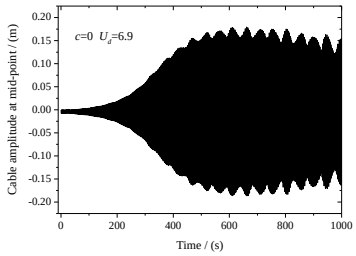

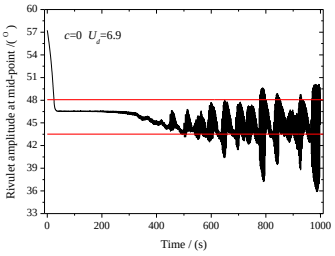

(a) c=0 N·s/m

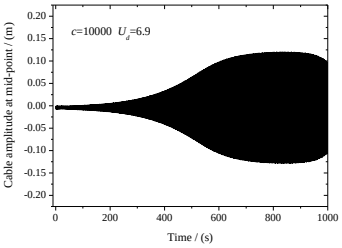

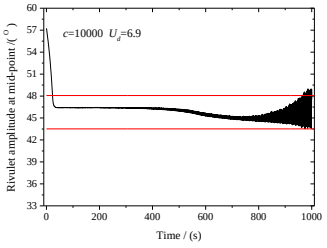

(b) c=1×104 N·s/m

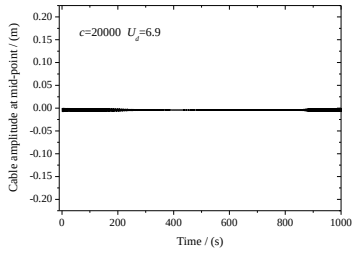

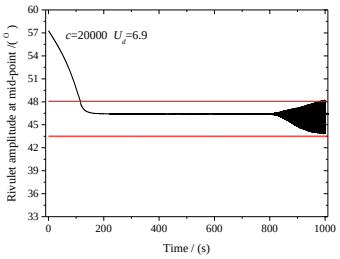

(c) c=2×104 N·s/m

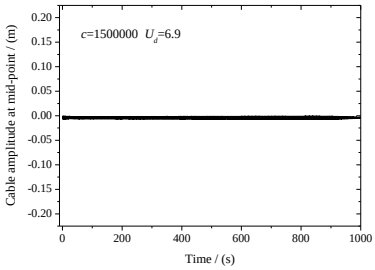

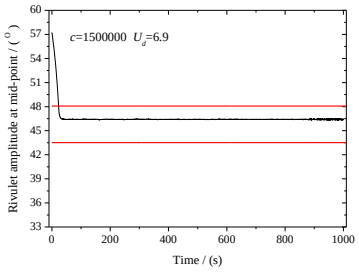

(d) c=1.5×106 N·s/m

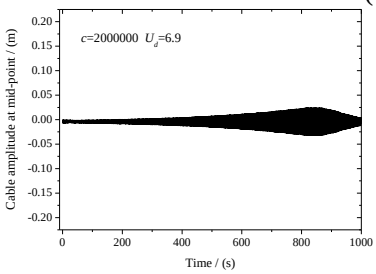

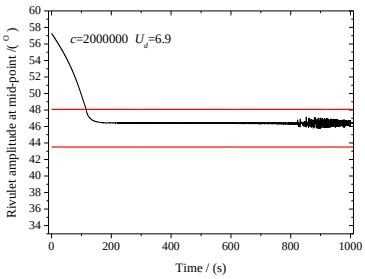

(e) c=2×106 N·s/m

Fig. 16 Timehistories of cable and rivulet diplacements at mid-point of the cable for U_d=6.9 m/s

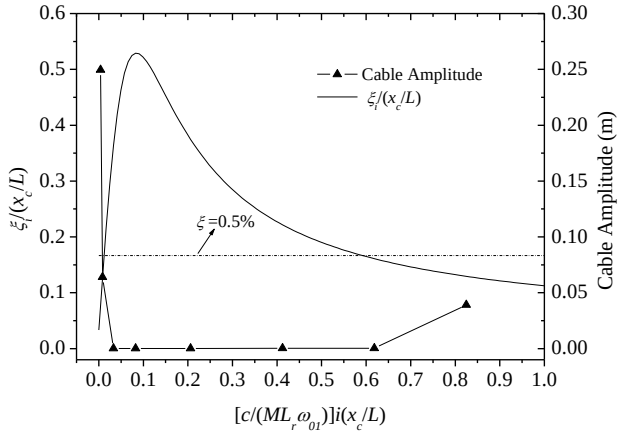

Fig. 17 The relationship between the cable amplitude and damping coefficient of the dampers (U_d=6.9 m/s)

Fig. 16 presents the time histories of cable and rivulet displacements at the mid-point of the cable for U_d=6.9 m/s when c=0, 1×104, 2×104, 1.5×106 and 2×106 N·s/m. A sudden decrease of aerodynamic force coefficient of the cable with the rivulet arises within the two red horizontal lines in Fig. 16 (Gu 2009, Li, Chen *et al*. 2013). Energy from the approaching flow will be transferred into the cable vibration if the rivulet moves into the sudden decrease region, for example, when U_d=6.9 m/s as indicated in Fig. 16. It could be found from Figs. 16(a) and 16(b) that the oscillation of the rivulet is evoked after the amplitude of the cable arrives at its maximum value, which means that the cable oscillation is the key factor for the rivulet oscillation. On the other hand, the oscillation of the rivulet, which makes it intermittently moves out of the sudden decrease region of the aerodynamic force coefficient, appears to reduce the oscillation amplitude of the cable. If the dampers installed at the end of the cable could absorb enough energy from the cable oscillation, the cable oscillation would be well mitigated, as indicated in Figs. 16(c) and 16(d). The combination effects of the energy injection due to the negative aerodynamic damping (when rivulet moves into the sudden decrease region) and the energy extraction due to the installed dampers on the cable vibration system results in the final state of the stay cables.

Fig. 17 presents the relationship between the cable amplitude and damping coefficient of the dampers for U_d=6.9 m/s, together with the damping ratio curve. From Fig. 17, it could be concluded that the RWIV oscillation of stay cable is well mitigated if the realizable damping ratio is larger than 0.5%. This agrees well with the results of Virlogeux (1999) and Chen, Wang *et al*. (2004), which were obtained from field observations. Virlogeux (1999) pointed out that a damping ratio of 0.5% was enough to alleviate the RWIV of stay cable. The stay cables on Dongting Lake Bridge were well mitigated through a realizable damping ratio of 0.5~1.2%, which is provided by MR dampers near the bridge deck.

In order to analyze the mechanism of the dampers to reduce cable vibration, Fig. 18 shows the cable oscillation profile for different damping coefficient of the dampers, including c=1×104, 2×105, 2×106 and 2×107 N·S/m2, which correspond to modal damping ratio of 0.24%, 1.53%, 0.39%, 0.13%, respectively. If the damping coefficient of the dampers is small, for example c=1×104 N·S/m2, the achievable damping force provided by the dampers is so small that it has little effects on the cable oscillation profile, as indicated in Fig. 18(a). If the damping coefficient is

large enough, for example c=2×107 N·S/m2, the cable oscillation do not evoke the motion of the dampers, which makes the point where the dampers are installed as a fixed point, as indicated in Fig. 18(d). In this case, the role of the dampers is to shorten the cable by the percentage of x_c/L. If the optimal damping coefficient, c=2×105 N·S/m2, is used, a medium size of damping force of the dampers are cable of dissipating considerable energy, which offer a large damping ratio and reduce the cable oscillation, as indicated in Fig. 18(b).

5. Conclusions

The effectiveness of dampers to RWIVs of stay cables is numerically analyzed by means of FDM. As is well-known, the concentrated damping coefficient provided by the dampers implies an infinite damping coefficient at the location where the dampers are installed. Hence, the concentrated damping coefficient is simplified by five types of distributed damping coefficients, including 3-points triangle, 5-points triangle, 5-points trapezoid, 3-points cosine and 5-points cosine, which could be easily implemented in FDM. A taut string model attached with a damper is adopted to carry out free vibration analysis to validate the accuracy of these distributed damping coefficients. Comparing with the classic results proposed by Pacheco and Fujino (1993), it appears that the distributed damping coefficient of 3-points triangle offers the best approximation for the concentrated damping coefficient.

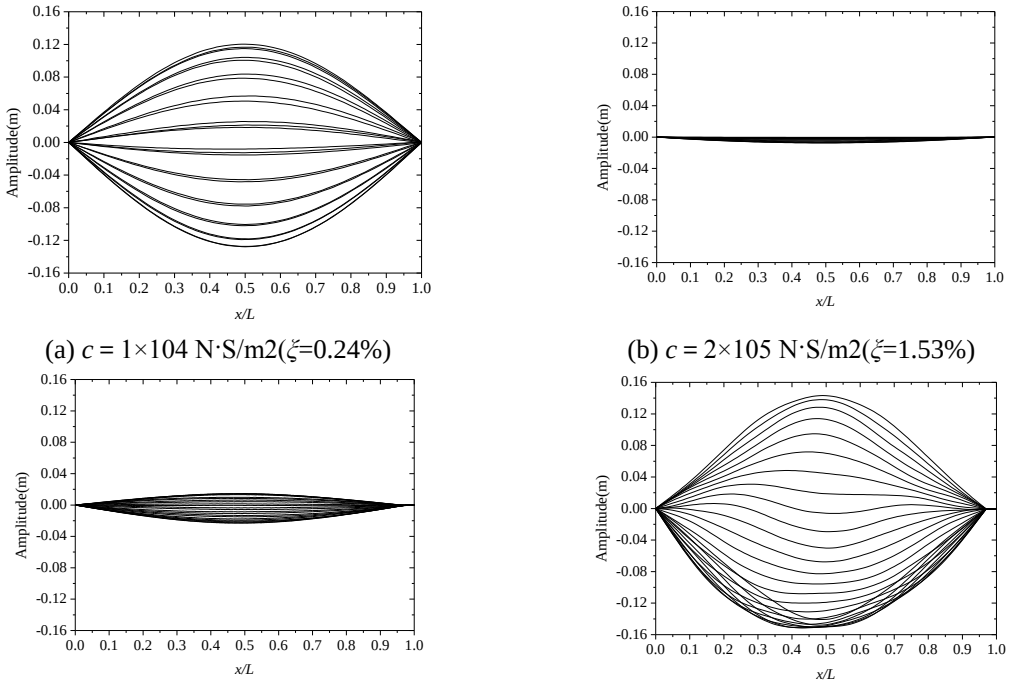

(a) c = 1×104 N·S/m2(ξ=0.24%) (b) c = 2×105 N·S/m2(ξ=1.53%)

(c) c = 2×106 N·S/m2(ξ=0.39%) (d) c = 2×107 N·S/m2(ξ=0.13%)

Fig. 18 The cable oscillation profile for different damping coefficient of the dampers

Free vibration analysis of a 3-D continuous stay cable attached with two dampers are carried out to obtain the modal damping ratio provided by the dampers. The effects of the orientation of the dampers and cable sag on the modal damping ratio are investigated in detail. The results show that the orientation of the dampers has no significant effects on the realizable maximum damping ratio, however, the corresponding optimal damping coefficient of the damper is different for various orientations of the dampers. On the other hand, cable sag has significant effects on the realizable maximum damping ratio of the first mode. The larger of the cable sag ratio, the lower of the realizable maximum damping ratio can be obtained. Fortunately, the realizable maximum damping ratio of the first mode for a normal cable sag ratio, for example, 0.6%, is nearly identical with the value of a taut string.

Based on the theoretical model developed by Gu (2009), the RWIV response of a 3-D continuous stay cable attached with two dampers is computed by means of FDM. The effectiveness of the dampers for mitigating the RWIVs of stay cables is discussed. The results show that the RWIV oscillation of stay cable could be well mitigated by the dampers, and it seems that 0.5% of damping ratio is sufficient to reduce the RWIV vibration.

Acknowledgements

This project was jointly supported by the National Basic Research Program of China (973 Program: 2015CB057701 and 2015CB057702), the National Natural Science Foundation (50708035), the China Postdoctoral Science Foundation (20060400873), to which the authors gratefully appreciate.

References

Bosdogianni, A. and Olivari, D. (1996), "Wind- and rain-induced oscillations of cables of stayed bridges", *J. Wind Eng. Ind. Aerod.*, **64**(2-3), 171-185.

Cao, D.Q., Tucker, R.W. and Wang, C. (2003), "A stochastic approach to cable dynamics with moving rivulets", *J. Sound Vib.*, **268**(2), 291-304.

Chen, Z.Q., Wang, X.Y., Ko, J.M., Ni, Y.Q., Yang, G. and Hu, J.H. (2004), "MR damping system for mitigating wind-rain induced vibration on Dongting Lake cable-stayed bridge", *Wind Struct.*, **7**(5), 293-304.

Cheng, S.H., Irwin, P.A. and Tanaka, H. (2008b), "Experimental study on the wind-induced vibration of a dry inclined cable-Part II: Proposed Mechanisms", *J. Wind Eng. Ind. Aerod.*, **96**(12), 2254-2272.

Cheng, S.H., Larose, G.L., Savage, M.G., Tanaka, H. and Irwin, P.A. (2008a), "Experimental study on the wind-induced vibration of a dry inclined cable-Part I: Phenomena", *J. Wind Eng. Ind. Aerod.*, **96**(12), 2231-2253.

Cosentino, N., Flamand, O. and Ceccoli, C. (2003), "Rain-wind induced vibration of inclined stay cables. Part II: Mechanical modeling and parameter characterization", *Wind Struct.*, **6**(6), 485-498.

Du, X.Q., Gu, M. and Chen, S.R. (2013), "Aerodynamic characteristics of an inclined and yawed circular cylinder with artificial rivulet", *J. Fluid. Struct.*, **43**, 64-82.

Flamand, O. (1995), "Rain-wind induced vibration of cables", *J. Wind Eng. Ind. Aerod.*, **57**(2-3), 353-362.

Fujino, Y. and Hoang, N. (2008), "Design formulas for damping of a stay cable with a damper", *J. Struct. Eng.- ASCE*, **134**(2), 269-278.

Gu, M. (2009), "On wind–rain induced vibration of cables of cable-stayed bridges based on quasi-steady assumption", *J. Wind Eng. Ind. Aerod.*, **97**(7-8), 381-391.

Gu, M. and Du, X. Q. (2005), "Experimental investigation of rain-wind-induced vibration of cables in cable-stayed bridges and its mitigation", *J. Wind Eng. Ind. Aerod.*, **93**(1), 79-95.
Gu, M. and Lu, Q. (2001), "Theoretical analysis of wind-rain induced vibration of cables of cable-stayed bridges", *Proceedings of the 5th Asia-Pacific Conf. on Wind Engineering*, Japan Association for Wind Engineering, Kyoto, Japan.
Gu, M., Du, X.Q. and Li, S.Y. (2009), "Experimental and theoretical simulations on wind–rain-induced vibration of 3-D rigid stay cables", *J. Sound Vib.*, **320**(1-2), 184-200.
Hikami, Y. and Shiraishi, N. (1988), "Rain-wind induced vibrations of cables in cable stayed bridges", *J. Wind Eng. Ind. Aerod.*, **29**(1-3), 409-418.
Krenk, S. (2000), "Vibrations of a taut cable with an external damper", *J. Appl. Mech. -T ASME*, **67**, 772-776.
Li, F.C., Chen, W. L., Li, H. and Zhang, R. (2010), "An ultrasonic transmission thickness measurement system for study of water rivulets characteristics of stay cables suffering from wind-rain-induced vibration", *Sensor. Actuat. - A Phys.*, **159**(1), 12-23.
Li, S.Y. and Gu, M. (2006), "Numerical simulations of flow around stay cables with and without fixed artificial rivulets", *Proceedings of the 4th International Symposium on Computational Wind Engineering (CWE2006)*, Yokohama, Japan.
Li, S.Y., Chen, Z.Q., and Li, S.K. (2014), "Theoretical investigation on rain-wind induced vibration of a continuous stay cable with given rivulet motion", *Wind Struct.*, **19**(5), 481-503.
Li, S.Y., Chen, Z.Q., Wu, T. and Kareem, A. (2013), "Rain-wind induced in-plane and out-of-plane vibrations of stay cables", *J. Eng. Mech. - ASCE*, **139**(12), 1688-1698.
Main, J.A. and Jones, N.P. (2002), "Free vibrations of taut cable with attached damper I: Linear viscous damper", *J. Eng. Mech. - ASCE*, **128**(10), 1062-1071.
Main, J.A. and Jones, N.P. (2007), "Vibration of tensioned beams with intermediate viscous damper II: Damper near a support", *J. Eng. Mech.- ASCE*, **133**(4), 379-388.
Matsumoto, M., Saitoh, T., Kitazawa, M., Shirato, H. and Nishizaki, T. (1995), "Response characteristics of rain-wind induced vibration of stay-cables of cable-stayed bridges", *J. Wind Eng. Ind. Aerod.*, **57**(2-3), 323-333.
Matsumoto, M., Shirato, H., Yagi, T., Goto, M., Sakai, S. and Ohya, J. (2003), "Field observation of the full-scale wind induced cable vibration", *J. Wind Eng. Ind. Aerod.*, **91**(1-2), 13-26.
Matsumoto, M., Yagi, T., Shigemura, Y. and Tsushima, D. (2001), "Vortex-induced cable vibration of cable-stayed bridges at high reduced wind velocity", *J. Wind Eng. Ind. Aerod.*, **89**(7-8), 633-647.
Pacheco, B.M., Fujino, Y. and Sulekh, A. (1993), "Estimation curve for modal damping in stay cables with viscous damper", *J. Struct. Eng.- ASCE*, **119**(6), 1061-1079.
Peil, U. and Nahrath, N. (2003), "Modeling of rain-wind induced vibrations", *Wind Struct.*, **6**(1), 41-52.
Phelan, R.S., Sarkar, P.P. and Mehta, K.C. (2006), "Full-scale Measurements to investigate rain-wind induced cable-stay vibration and its mitigation", *J. Bridge Eng.*, **11**(3), 293-304.
Robertson, A.C., Taylor, I.J., Wilson, S.K., Duffy, B.R. and Sullivan, J.M. (2010), "Numerical simulation of rivulet evolution on a horizontal cable subject to an external aerodynamic field", *J. Fluid. Struct.*, **26**, 50-73.
Tabatabai, H. and Mehrabi, A.B. (2000), "Design of mechanical viscous dampers for stay cables", *J. Bridge Eng.*, **5**(2), 114-123.
Tikhonov, A.N. and Samarskii, A.A. (1963), "Equations of mathematical physics", *Dover Publications, INC.*, New York.
van der Burgh, A.H.P. and Hartono (2004), "Rain-wind-induced vibrations of a simple oscillator", *Int. J. Nonlinear Mech.*, 39(1), 93-100.
Virlogeux, M. (1998), "Cable vibrations in cable-stayed bridges", In *Bridge Aerodynamics*, Balkema, Rotterdam, 213-233.
Wang, Z.J., Zhou Y., Huang, J.F. and Xu Y.L. (2005), "Fluid dynamics around an inclined cylinder with running water rivulets", *J. Fluid. Struct.*, **21**, 49-64.
Wilde, K. and Witkowski, W. (2003), "Simple model of rain-wind-induced vibrations of stayed cables", *J.*

Wind Eng. Ind. Aerod., **91**, 873-891.
Wu, T., Kareem, A. and Li, S.Y. (2013), "On the excitation mechanisms of rain–wind induced vibration of cables: Unsteady and hysteretic nonlinear features", *J. Wind Eng. Ind. Aerod.*, **122**, 83-95.
Xu, Y.L. and Wang, L.Y. (2003), "Analytical study of wind-rain-induced cable vibration: SDOF model", *J. Wind Eng. Ind. Aerod.*, **91**(1-2), 27-40.
Xu, Y.L. and Yu, Z. (1998), "Mitigation of three-dimensional vibration of inclined sag cable using discrete oil dampers - II. Application", *J. Sound Vib.*, **214**(4), 675-693.
Yamaguchi, H. (1990), "Analytical study on growth mechanism of rain vibration of cables", *J. Wind Eng. Ind. Aerod.*, **33**(1-2), 73-80.
Yamaguchi, H. and Fujino, Y. (1998), "Stayed cable dynamics and its vibration control", In *Bridge Aerodynamics*, Balkema, Rotterdam, 235-253.
Yu, Z. and Xu, Y.L. (1998), "Mitigation of three-dimensional vibration of inclined sag cable using discrete oil dampers - I. Formulation", *J. Sound Vib.*, **214**(4), 659-673.
Zuo, D., Jones, N.P. and Main, J.A. (2008), "Field observation of vortex- and rain-wind-induced stay-cable vibrations in a three-dimensional environment", *J. Wind Eng. Ind. Aerod.*, **96**(6-7), 1124-1133.

CC